TECHNICAL NOTE

Estimating Unknown Input Parameters when Implementing the NGA Ground-Motion Prediction Equations in Engineering Practice

James Kaklamanos,[a) S.M.EERI, **Laurie G. Baise,[a)** M.EERI, **and David M. Boore[b)**

The ground-motion prediction equations (GMPEs) developed as part of the Next Generation Attenuation of Ground Motions (NGA-West) project in 2008 are becoming widely used in seismic hazard analyses. However, these new models are considerably more complicated than previous GMPEs, and they require several more input parameters. When employing the NGA models, users routinely face situations in which some of the required input parameters are unknown. In this paper, we present a framework for estimating the unknown source, path, and site parameters when implementing the NGA models in engineering practice, and we derive geometrically-based equations relating the three distance measures found in the NGA models. Our intent is for the content of this paper not only to make the NGA models more accessible, but also to help with the implementation of other present or future GMPEs. [DOI: 10.1193/1.3650372]

INTRODUCTION

Ground-motion prediction equations (GMPEs) are used to estimate the ground motion at a given location as a function of earthquake magnitude, distance from the earthquake source, and other source, path, and site characteristics. Douglas (2003) provides an excellent review of existing GMPEs and the variables associated with them. In 2008, five new GMPEs were released as part of the Next Generation Attenuation of Ground Motions ("NGA-West," or "NGA") project, coordinated by the Pacific Earthquake Engineering Research Center (PEER). The NGA models predict peak ground acceleration (PGA), peak ground velocity (PGV), and 5%-damped pseudo-absolute response spectral acceleration (PSA) for shallow crustal earthquakes in active tectonic regions, such as California (Abrahamson and Silva 2008, "AS08"; Boore and Atkinson 2008, "BA08"; Campbell and Bozorgnia 2008, "CB08"; Chiou and Youngs 2008a, "CY08"; Idriss 2008, "I08"). Numerous researchers have found that the NGA models may be applied, sometimes following minor adjustment, to other tectonic regions, such as Iran (Ghasemi et al. 2008, Shoja-Taheri et al. 2010) and Europe

[a) Department of Civil and Environmental Engineering, 113 Anderson Hall, Tufts University, Medford, MA 02155

[b) Earthquake Science Center, U.S. Geological Survey, Mail Stop 977, 345 Middlefield Road, Menlo Park, CA 94025

Table 1. Input parameters of the NGA models (modified from Kaklamanos and Baise 2011)

Parameter	Model				
	AS08	BA08	CB08	CY08	I08
Source parameters:					
Moment magnitude, $\mathbf{M}$	●	●	●	●	●
Depth-to-top of rupture, Z_{TOR}	●		●	●	
Down-dip rupture width, W	●				
Fault dip, δ	●		●	●	
Style-of-faulting flag (function of rake angle, λ)	●	●	●	●	●
Aftershock flag (for models applicable to aftershocks)	●			●	
Path parameters:					
Closest distance to the rupture plane (rupture distance), R_{RUP}	●		●	●	●
Horizontal distance to the surface projection of the rupture (Joyner-Boore distance), R_{JB}	●	●	●	●	
Horizontal distance to top edge of rupture measured perpendicular to the strike (site coordinate), R_X	●			●	
Hanging-wall flag	●			●	
Site parameters:					
Time-averaged shear-wave velocity over the top 30 meters of the subsurface, V_{S30}	●	●	●	●	
Depth to $V_S = 1.0$ km/s ($Z_{1.0}$)	●			●	
Depth to $V_S = 2.5$ km/s ($Z_{2.5}$)	●		●		
PGA (or PSA) on rock, as baseline for nonlinear site response	●	●	●	●	

(Campbell and Bozorgnia 2006, Scasserra et al. 2009, Stafford et al. 2008). Thus, these GMPEs are beginning to have an impact on seismic hazard analyses worldwide.

Although the new NGA models have significantly higher prediction accuracies than their predecessors (as quantified by Kaklamanos and Baise 2011), they are also significantly more complicated. As seen in Table 1, which displays the input parameters for the five NGA models, they vary significantly in terms of complexity and number of predictor variables. Kaklamanos and Baise (2011) find that the more complex NGA models (those with more input parameters and more complexity of functional forms) do not have a predictive advantage over the simpler NGA models in many situations because the values of several input parameters are often unknown. When implementing the NGA models, users are faced with the challenge of estimating unknown input parameters, for some of which there is limited guidance in the literature. In this paper, we present a clear framework for estimating the source, path, and site parameters when applying the NGA models. Our framework requires the user to specify a bare minimum of five values:

- Moment magnitude, $\mathbf{M}$
- Joyner-Boore distance, R_{JB}
- Time-averaged shear-wave velocity over a subsurface depth of 30 meters, V_{S30}

- Style of faulting (e.g., rake angle, λ)
- Hanging-wall flag, F_{HW}

The remaining input parameters may be estimated by the methods described in this paper. It is important to note that by the laws of error propagation, uncertainties in the predictor variables (source, path, and site) are transmitted to the ground motion estimate. Assume that x appears as an input parameter in a relationship for estimating y; in a strict sense, if an empirical correlation with standard deviation σ_x is used to estimate x, then the standard deviation of y will be represented by σ_{total}, modified from σ_y by:

$$\sigma_{total} = \sqrt{\sigma_y^2 + \left(\frac{\partial y}{\partial x}\right)^2 \sigma_x^2}. \tag{1}$$

In GMPEs, for which the total standard deviation is determined in natural logarithmic space, y in the above equation would be $\ln(PGA)$, $\ln(PGV)$, or $\ln(PSA)$. One advantage of having more complex GMPEs with many input parameters is lower aleatory variabilities (sigmas), but these lower sigmas are inappropriate if the input parameters are unknown, because the uncertainties of the estimated input parameters will propagate into the uncertainty of the estimated ground motion. For each NGA model, however, the developers incorporated typical uncertainties of earthquake source, path, and site processes into the estimates of aleatory variability. A full analysis and discussion of error propagation is beyond the scope of this technical note. Bommer et al. (2005) provide an excellent discussion on the effects of conversions of predictor variables on the aleatory variability of GMPEs.

Kaklamanos et al. (2010) used the framework introduced in this paper for their implementations of the NGA models in the programming languages Fortran and R (R Development Core Team 2011). In this paper, we describe the selected methods of estimation in Kaklamanos et al. (2010) and present alternatives to those selected methods. First, we offer recommendations for estimating the source characteristics describing the fault rupture plane: the fault dip (δ), down-dip rupture width (W), and depth-to-top of rupture (Z_{TOR}). Secondly, we derive physically based equations that relate the three distance measures used in the NGA models: (1) the slant distance to the closest point on the rupture plane (the rupture distance, R_{RUP}), (2) the horizontal distance to the surface projection of the rupture (the Joyner-Boore distance, R_{JB}), and (3) the horizontal distance to the surface projection of the top edge of the rupture measured perpendicular to the fault strike (the site coordinate, R_X). These equations will be useful for situations in which the geometric coordinates of the fault rupture are not pre-determined, and for checking for consistency between the various distance measures. The vertical cross section in Figure 1 illustrates the three distance measures and three rupture parameters for a hypothetical site. We also compare our physical equations to alternative empirical methods for estimating the distance parameters. Finally, we summarize methods of estimating the site parameters required in addition to V_{S30}: the soil depth parameters $Z_{1.0}$ (depth to $V_S = 1.0$ km/s, used in AS08 and CY08) and $Z_{2.5}$ (depth to $V_S = 2.5$ km/s, used in CB08). Our intent is for the content of this paper to make the NGA models more accessible to earthquake engineering practitioners. Additionally, this framework may help with the implementation of other present or future GMPEs for seismic hazard analyses.
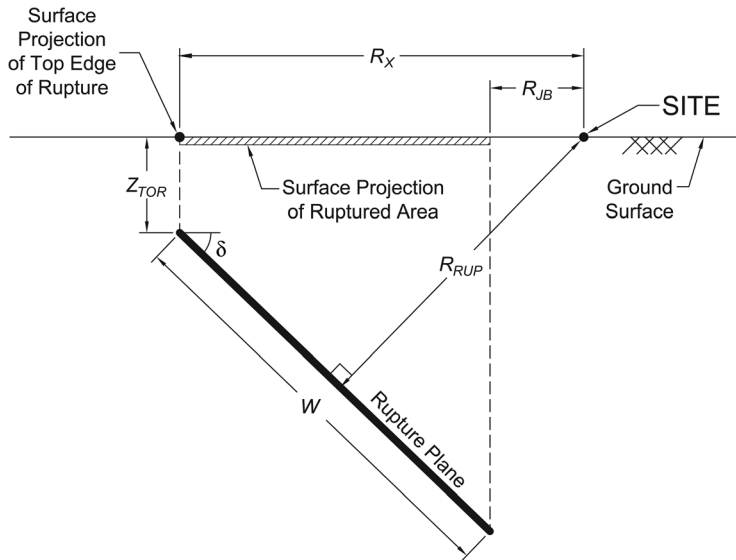
Figure 1. Illustration of earthquake source and distance measures using a vertical cross section through a fault rupture plane. The length of the fault rupture plane (L) is measured along the strike (perpendicular to the plane of the page).

ESTIMATION OF SOURCE PARAMETERS

The fault dip, down-dip rupture width, and depth-to-top of rupture are often unknown for historical earthquakes without finite fault models, and for various earthquake scenarios in seismic hazard analyses. Here, we offer recommendations for estimating these rupture parameters from the earthquake magnitude and style of faulting. First, however, we provide a clarification on how the different NGA models classify style of faulting by the rake angle for an event. A summary of the style-of-faulting classifications for the five NGA models is presented in Table 4 of Abrahamson et al. (2008). However, there are some ambiguities when this is compared to the individual papers, with regards to some inequalities being open or closed. In the implementation of Kaklamanos et al. (2010), these ambiguities were reconciled by following the style-of-faulting recommendations in the individual papers (superseding Abrahamson et al. 2008, where there is conflicting information), and we present the summary in Table 2 in this paper. For example, for an event with $\lambda = 30°$, CB08 differs from the other models in classifying the event as strike-slip instead of reverse. If the style of faulting is known but the value of λ is not, the user may assume generic rake angles of $90°$ for reverse events, $-90°$ for normal events, $0°$ for left-lateral strike-slip events, and $180°$ for right-lateral strike-slip events (although GMPEs make no distinction between left-lateral and right-lateral strike-slip events).

FAULT DIP ANGLE, δ

For faults with sufficient geologic data and/or previous seismic activity, this supplemental information may be used to make a reasonable assumption for the dip angle (δ). When δ cannot be specified, it may be estimated from the style of faulting (using the rake angle) with the

Table 2. NGA style-of-faulting classifications

Model	Reverse faulting	Normal faulting	Strike-slip faulting
		Range of rake angles (deg)	
AS08	$30 \leq \lambda \leq 150$	$-120 \leq \lambda \leq -60$	$-180 < \lambda < -120, -60 < \lambda < 30$, and $150 < \lambda < 180$
BA08	$30 \leq \lambda \leq 150$	$-150 \leq \lambda \leq -30$	$-180 < \lambda < -150, -30 < \lambda < 30$, and $150 < \lambda < 180$
CB08	$30 < \lambda < 150$	$-150 < \lambda < -30$	$-180 \leq \lambda \leq -150, -30 \leq \lambda \leq 30$, and $150 \leq \lambda \leq 180$
CY08	$30 \leq \lambda \leq 150$	$-120 \leq \lambda \leq -60$	$-180 < \lambda < -120, -60 < \lambda < 30$, and $150 < \lambda < 180$
I08	$30 \leq \lambda \leq 150$	N/A	$-180 < \lambda < 30$ and $150 < \lambda < 180$

following guidelines, modified from the approach given in Chiou and Youngs (2008b). Following standard practice, strike-slip faults are assumed to be vertical ($\delta = 90°$). Average values are recommended for normal faulting events ($\delta = 50°$) and reverse faulting events ($\delta = 40°$). The recommendation for normal faulting events comes from an analysis of the normal faulting earthquakes in the NGA flatfile and the worldwide compilations by Collettini and Sibson (2001) and Jackson and White (1989), as well as events in the Finite-Source Rupture Model Database (Mai 2007). For reverse faulting earthquakes, Sibson and Xie (1998) find that the fault dip distribution is bimodal, with one peak near 30° and a subsidiary peak near 50°, with an average dip angle in the range of 40°. Our recommendation is consistent with the findings of Sibson and Xie (1998) and the approach of Chiou and Youngs (2008b), and our recommended dip angle is close to that of the reverse faulting events in the NGA flatfile (43.5°).

DOWN-DIP RUPTURE WIDTH, W

The down-dip rupture width (W) may be estimated from the moment magnitude and style of faulting, using the relationships found in Table 2A in Wells and Coppersmith (1994):

$$W = \begin{cases} 10^{-0.76+0.27\mathbf{M}} & \text{for strike-slip events} \\ 10^{-1.61+0.41\mathbf{M}} & \text{for reverse events} \\ 10^{-1.14+0.35\mathbf{M}} & \text{for normal events.} \end{cases} \tag{2}$$

Given the size of the regression database and the statistical robustness of the relationships, the Wells and Coppersmith (1994) empirical equations are a reasonable method for estimating W.

DEPTH-TO-TOP OF RUPTURE, Z_{TOR}

Little guidance exists in the literature on the estimation of Z_{TOR}. The method employed in Kaklamanos et al. (2010) is to estimate Z_{TOR} from the hypocentral depth (Z_{HYP}), down-dip rupture width (W), and dip (δ), assuming that the hypocenter is located 60% down the fault width, as suggested by the results of Mai et al. (2005):

$$Z_{TOR} = \max[(Z_{HYP} - 0.6W \sin \delta), 0]. \tag{3}$$

The values of W and δ may be estimated using the aforementioned methods, and Z_{HYP} may be estimated using the linear relationship between Z_{HYP} and $\mathbf{M}$ published in Table 1 of Scherbaum et al. (2004):

$$Z_{HYP} = \begin{cases} 5.63 + 0.68\mathbf{M} & \text{for strike-slip faulting} \\ 11.24 - 0.2\mathbf{M} & \text{for non-strike-slip faulting} \\ 7.08 + 0.61\mathbf{M} & \text{for general (unspecified) faulting} \end{cases} \tag{4}$$

We assume strike-slip events to have rake angles within $30°$ of horizontal; the general equation may be applied for borderline cases. Due to differences in the stress fields leading to rupture, dipping faults tend to have ruptures that originate deeper in the earth than strike-slip faults. For larger-magnitude earthquakes, there is an increase in the amount of energy released and the size of the rupture. To accommodate a larger rupture area, hypocenters of strike-slip events must become progressively deeper as the magnitude increases. The hypocentral depths of dip-slip and strike-slip events become more similar as $\mathbf{M}$ increases.

ESTIMATION OF DISTANCE PARAMETERS

Using various geometric principles, we derive physical equations relating the three distance measures required to implement the NGA models. GMPEs developed prior to the NGA project generally included just one type of distance parameter per model, so the issues of geometrical consistency are not an issue for these models. For models with multiple distance parameters (AS08, CB08, and CY08), the geometrical interdependence of the distance parameters is a phenomenon that must be considered in model implementation, especially at small distances; otherwise, considerable errors in ground-motion prediction can result. Our equations will be useful for implementing the NGA and other GMPEs in seismic hazard analyses and in research using historical earthquake datasets (such as the NGA flatfile used for GMPE development), which may not have information on new distance measures such as R_X. Little has been written in the literature about R_X, which is used in the AS08 and CY08 models for quantifying the hanging-wall effect. There is no clear published description on the physical relationship between R_X and the other distance parameters. Spudich and Chiou (2008) define a generalized geometry for multisegment ruptures, but they do not provide an explicit formulation for R_X.

To derive our distance equations, we must define an important location measure, the source-to-site azimuth (α). Figure 2 is a plan view of the surface projection of the ruptured area, and the surface projection of the top edge of rupture, which aligns with the fault strike. The positive y-axis is directed along the fault strike such that the ruptured area is to the right. The positive x-axis is in the direction of the ruptured area (the hanging-wall side of the fault). The source-to-site azimuth (α) for a given site is the angle between the positive fault strike direction and the line connecting the site to the closest point on the surface projection of the top edge of rupture, with clockwise angles assumed positive (Chiou 2005). Sites located on the hanging wall have positive azimuths (ranging from $0°$ to $180°$), and sites located on the footwall have negative azimuths (ranging from $-180°$ to $0°$). R_X is defined to be positive for sites on the hanging-wall side of the fault and negative for sites on the footwall side of the fault (Chiou and Youngs 2008a). As Figure 3 illustrates, a site can be categorized into one of nine cases, based (1) on the value of α, and (2) on some additional specifications on how the site is oriented with respect to the ruptured area (for sites on the hanging-wall side of the fault).

Our equations are derived by characterizing the earthquake source by the geometric parameters W, Z_{TOR}, and δ, and characterizing the location of the site of interest by assuming
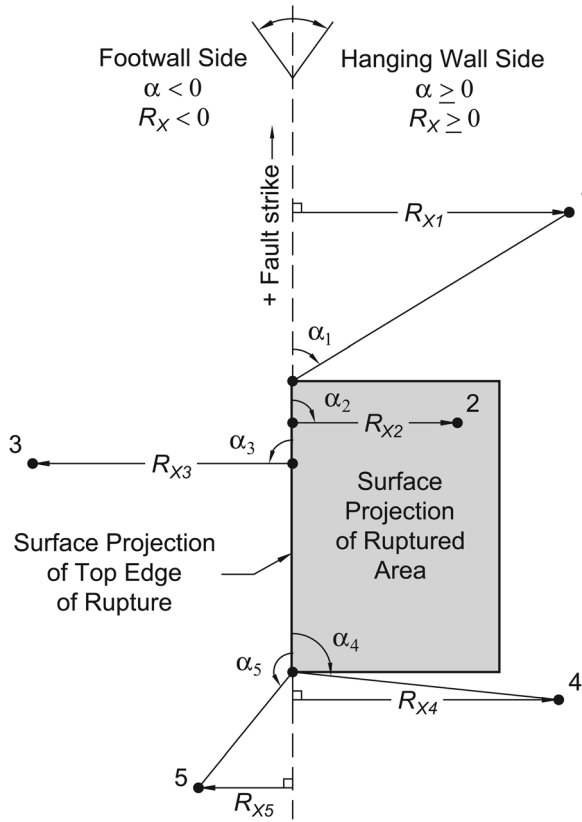
Figure 2. Plan view of a fault rupture, giving the definition and sign convention of the source-to-site azimuth (α). Also illustrated are five example sites and their source-to-site azimuths and site coordinates. Sites 1, 2, and 4, which are located on the hanging-wall side of the fault, have positive azimuths and site coordinates; sites 3 and 5, which are located on the footwall side of the fault, have negative azimuths and site coordinates.

R_{JB} and α. We use the Joyner-Boore distance (R_{JB}) as the primary distance measure because it is easily visualized in two dimensions as the horizontal distance to the surface projection of the rupture, and it can be thought of as an approximate epicentral distance. Therefore, if the user has only a generic source-to-site distance (R) for a ground-motion calculation, it is not unreasonable to use R_{JB} as the primary distance upon which others are computed. Given R_{JB}, α, and the source parameters W, Z_{TOR}, and δ (which may be estimated using the aforementioned methods in this paper), the other two distance parameters (R_{RUP} and R_X) are geometrically constrained. We start by deriving equations for R_X, and then derive equations for R_{RUP}. In practice, R_X can be calculated from R_{JB} and α, and then R_{RUP} can then be calculated from R_X. When the source-to-site distance envisioned by the user is a measure different than R_{JB}, numerical methods may be employed to backsolve for the distance measures in any order, provided that at least two parameters in the set $\{R_{RUP}, R_{JB}, R_X, \alpha\}$ are assumed. The computer programs made available by Kaklamanos (2010) allow for such solutions.
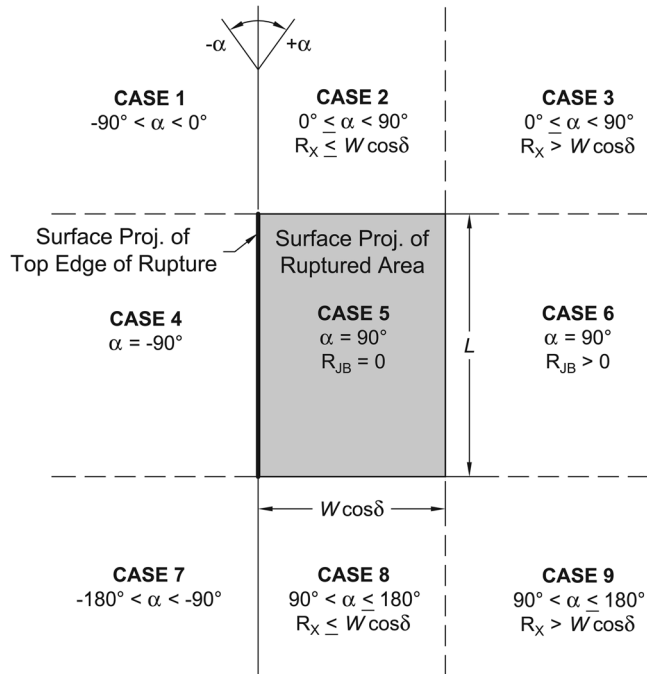
Figure 3. Plan view of the nine geometric cases for the location of a site with respect to the fault strike and surface projection of ruptured area, used in the calculation of R_X.

The one situation in which R_X and R_{RUP} are not constrained by R_{JB}, α, and the source parameters, is for $R_{JB} = 0$, in which the site is located directly above the ruptured area. In this situation, either R_X or R_{RUP} must be specified in addition to $R_{JB} = 0$ in order to calculate the third distance parameter. If neither R_X nor R_{RUP} can be assumed in this situation, then we suggest following the methodology of Kaklamanos et al. (2010) and assuming that the site is located in the middle of the surface projection of the ruptured area; that is,

$$R_X = \frac{1}{2} W \cos \delta. \tag{5}$$

One of the main challenges with implementing our distance equations is determining the source-to-site azimuth, which may not be known. If α is unknown, we recommend that α be $50°$ for sites on the hanging-wall side of the fault ($F_{HW} = 1$) and $-50°$ for sites on the foot-wall side of the fault ($F_{HW} = 0$). These numbers are approximations based upon the average values in the NGA flatfile ($48.5°$ for hanging wall sites and $-53.1°$ for footwall sites), and are used in Kaklamanos et al. (2010). The distance calculations are symmetric for sites reflected across a line perpendicular to the strike, passing through the center of the fault (mathematically, any site with an azimuth equal to $\text{sgn}(\alpha) \cdot (180° - \alpha)$ will have the same distance measures as a site with an azimuth of α). For example, a pair of sites with azimuths of $35°$ and $145°$ will have identical distance measures, as will a pair of sites with azimuths of $-50°$ and $-130°$. Therefore, in computing the average recommended azimuths for use,

azimuths with absolute values greater than $90°$ were reflected so that $0 \leq |\alpha| \leq 90°$. When the orientation of the site with respect to the fault rupture is not known, the rationale for using an average azimuth is to calculate distances for an intermediate case; i.e., to avoid bias in the calculation of the distance measures. Azimuths with a low value (e.g., $0°$) will place the site near the strike (resulting in a small R_X), and azimuths with a high value (e.g., $90°$) will place the site furthest from the strike (resulting in a large R_X). By using an average value for the azimuth, the resulting value of R_X represents an intermediate case—it is not clearly biased in a certain direction. Using the approach we have taken, the reality is that the numerical value of the azimuth for footwall sites does not matter; as long as α is negative, the value of α does not influence the calculated value of R_{RUP}. The calculated value of R_X is affected, but it does not enter the ground-motion calculations because the hanging-wall terms (which include R_X) are zero for footwall sites.

We make three key assumptions that do not greatly limit the situations to which our equations may be applied. First, we assume that the ruptured area is represented as a single plane. This is a reasonable proposition for the vast majority of earthquakes; for multisegment ruptures, our equations offer an approximate solution. Second, we neglect the effects of the Earth's curvature; for the distances at which the NGA models may be applied (up to 200 km from the earthquake source), the assumption of a flat earth makes an insignificant difference. Third, we do not explicitly include the effects of station elevation; we reasonably assume that differences in station elevation are negligible in relation to the horizontal distances involved in the ground-motion calculations. However, if users wish to incorporate station elevation into the distance calculations, they may use a modified depth-to-top of rupture, Z_{TOR}', given by the equation

$$Z_{TOR}' = \max(Z_{TOR} + \Delta Z_{EL}, 0),\qquad(6)$$

where Z_{TOR} is the original depth-to-top of rupture and ΔZ_{EL} is the elevation difference between the site of interest and the ground surface at the fault rupture. We constrain Z_{TOR} to be non-negative to be consistent with the derivation of our geometric equations and the manner in which the NGA relations are designed to receive Z_{TOR} as an input parameter.

EQUATIONS FOR SITE COORDINATE, R_X

For nonvertical faults ($\delta \neq 90°$), the resulting expressions for R_X are shown as Equations 7 to 12 in Table 3. The equations are derived using trigonometry for each of the nine cases; here, we briefly describe the derivations. For conciseness, equations for different cases are combined whenever possible, using algebraic simplification. (For example, the expressions $R_{JB} \tan \alpha$ for Case 2 and $R_{JB} \tan(180° - \alpha)$ for Case 8 are combined in Equation 7 by using the absolute value function, and the fact that $\tan(180° - \alpha)$ is equal to $-\tan \alpha$.) Note that the inequality $R_X \leq W \cos \delta$ is equivalent to $R_{JB} |\tan \alpha| \leq W \cos \delta$ (Equations 7 and 8); the latter formulation is used because the inequality $R_X \leq W \cos \delta$ cannot be computed prior to knowing the value of R_X. Equation 8 (valid for Cases 3 and 9) is derived by using the law of sines twice, on two adjacent triangles; the derivation is slightly different from the others because R_{JB} is no longer orthogonal to the surface projection of the ruptured area.

Plan-view geometry is used to derive every equation in the table except for Equations 10 and 11, which are derived using a vertical cross section through the rupture plane.

Table 3. Equations for calculating R_X; nonvertical faults

Azimuth angles	Additional specifications	Case(s) (Fig. 3)	Equation for R_X	Eqn. No.
$0° \leq \alpha < 90°$ and $90° < \alpha \leq 180°$	$R_{JB}|\tan\alpha| \leq W\cos\delta$	2, 8	$R_X = R_{JB}|\tan\alpha|$	(7)
	$R_{JB}|\tan\alpha| > W\cos\delta$	3, 9	$R_X = R_{JB}\tan\alpha\cos\left[\alpha - \sin^{-1}\left(\dfrac{W\cos\delta\cos\alpha}{R_{JB}}\right)\right]$	(8)
$\alpha = 90°$	$R_{JB} > 0$	6	$R_X = R_{JB} + W\cos\delta$	(9)
	$R_{JB} = 0$ and $R_{RUP} < Z_{TOR}\sec\delta$	5A	$R_X = \sqrt{R_{RUP}{}^2 - Z_{TOR}{}^2}$	(10)
	$R_{JB} = 0$ and $R_{RUP} \geq Z_{TOR}\sec\delta$	5B	$R_X = R_{RUP}\csc\delta - Z_{TOR}\cot\delta$	(11)
$-180° \leq \alpha < 0°$	—	1, 4, 7	$R_X = R_{JB}\sin\alpha$	(12)

Because $R_{JB} = 0$ for all locations directly above the ruptured area, the parameters in the vertical cross section (such as R_{RUP} and Z_{TOR}) are necessary to constrain R_X when $R_{JB} = 0$. Figure 4 illustrates the different possibilities for the location of the closest point on the rupture plane. Depending on the size and orientation of the rupture plane, sites located directly above the ruptured area will have their closest point on the rupture plane at the top of the rupture plane (Case 5A; Equation 10) or at some intermediate point on the rupture plane (Case 5B; Equation 11). The third scenario (Zone C), in which the closest point is located at the bottom of the rupture plane, arises in the calculation of R_{RUP}, presented in the next section.

For vertical strike-slip faults (i.e., $\delta = 90°$), a modification of the equations is necessary for numerical stability, because $\tan\delta$ is undefined when $\delta = 90°$. For all cases, the value of R_X reduces to the simple equation

$$R_X = R_{JB}\sin\alpha \quad (\text{for } \delta = 90°). \tag{13}$$

EQUATIONS FOR RUPTURE DISTANCE, R_{RUP}

For nonvertical faults ($\delta \neq 90°$), the rupture distance, R_{RUP}, can be calculated by the equations

$$R_{RUP} = \sqrt{(R_{RUP}')^2 + R_Y{}^2}, \text{ where} \tag{14}$$

$$R_{RUP}' = \begin{cases} \sqrt{R_X{}^2 + Z_{TOR}{}^2} & \text{for } R_X < Z_{TOR}\tan\delta \tag{15} \\ R_X\sin\delta + Z_{TOR}\cos\delta & \text{for } Z_{TOR}\tan\delta \leq R_X \leq Z_{TOR}\tan\delta + W\sec\delta \tag{16} \\ \sqrt{(R_X - W\cos\delta)^2 + (Z_{TOR} + W\sin\delta)^2} & \text{for } R_X > Z_{TOR}\tan\delta + W\sec\delta, \tag{17} \end{cases}$$
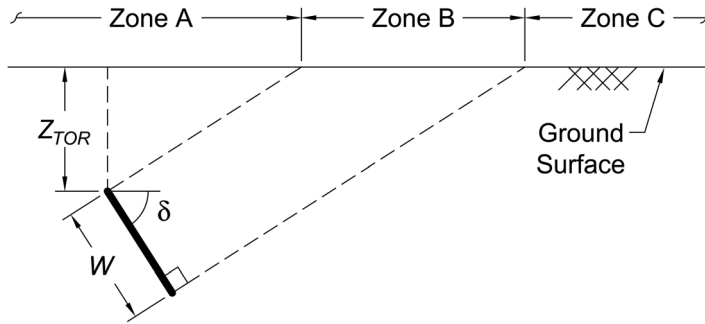
Figure 4. Vertical cross section illustrating the three categories to which a site may belong: Zone A, in which the closest distance from the site to the rupture plane is located at the top of the rupture plane; Zone B, in which the closest point on the rupture plane is located at an intermediate location along the plane; and Zone C, in which the closest point on the rupture plane is located at the bottom of the rupture plane.

$$\text{and} \quad R_Y = \begin{cases} 0 & \text{for } \alpha = \pm 90° & (18) \\ R_{JB} & \text{for } \alpha = 0° \text{ or } \pm 180° & (19) \\ |R_X \cot \alpha| & \text{otherwise.} & (20) \end{cases}$$

The in-plane rupture distance, R_{RUP}', is the closest distance to the rupture plane from a site aligned with the ruptured area in the x-direction ($\alpha = \pm 90°$; Cases 4, 5, and 6 in Figure 3). As illustrated in Figure 5, the distance R_Y is the closest distance from the site to the ruptured area, measured *parallel* to the strike; essentially, R_Y is the component of R_{JB} in the y-direction. Equations 15, 16, and 17, and the corresponding ranges of applicability for each equation, are derived using the geometry in Figure 4 for Zones A, B, and C, respectively. Note that Equation 15 is simply a rearrangement of Equation 10, and that Equation 16 is a rearrangement of Equation 11. The value of R_{RUP}' is equal to R_{RUP} for sites with $\alpha = \pm 90°$ (Equation 18), but for sites that are not aligned with the ruptured area in the x-direction, we must incorporate the distance R_Y by which the site is out-of-plane. The lengths R_{RUP}', R_Y, and R_{RUP} form a right triangle in which R_{RUP} (the desired quantity) is the hypotenuse, hence the calculation in Equation 14.

For vertical faults ($\delta = 90°$), the closest distance from a site to the rupture plane will always be located at the top of the rupture plane. For simplicity and numerical stability, the following equation should be used for vertical faults:

$$R_{RUP} = \sqrt{R_{JB}{}^2 + Z_{TOR}{}^2} \quad (\text{for } \delta = 90°). \tag{21}$$

EMPIRICAL RELATIONSHIPS BETWEEN DISTANCE MEASURES

Using simulated source geometries, Scherbaum et al. (2004) (termed "SSC04" here) developed expressions for converting source-to-site distance measures. The conversion equations are in the form of polynomial functions of **M**, R_{JB}, and style of faulting. An equation for R_{RUP} is available, but no equation for R_X is available (because R_X had not yet been introduced as a distance measure in 2004). SSC04 were the first to comprehensively address the
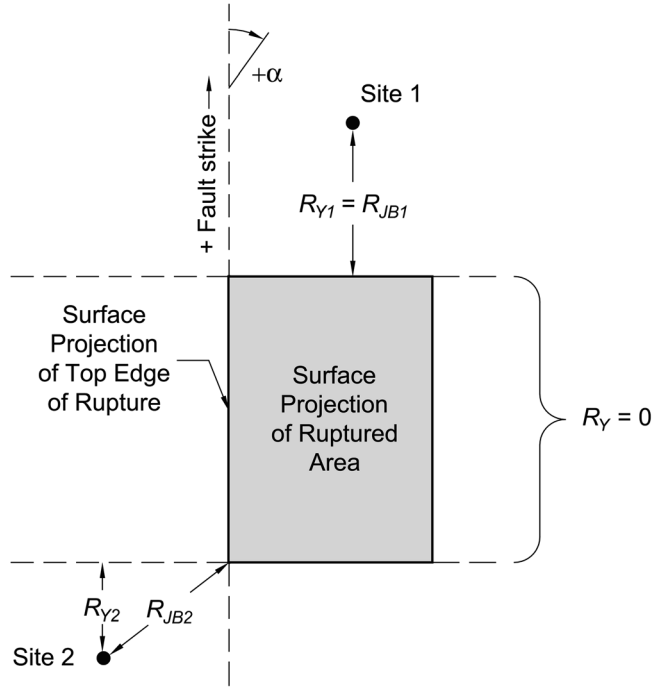
Figure 5. Plan view illustrating the definition of R_Y (used in the calculation of R_{RUP}), which is the distance from the site to the surface projection of the ruptured area, measured parallel to the strike. The distance, which is equal to zero for sites aligned with the ruptured area in the x-direction, can be considered to be the y-component of R_{JB}. Examples of R_Y for two sites are shown.

issue of distance conversions, and although their approach is different from ours, the SSC04 equations are a viable alternative to the physical equations we have presented for estimating R_{RUP}. For $n = 2{,}843$ records in the NGA flatfile (PEER 2008) with finite fault models, we estimated R_{RUP} using both our framework and that of SSC04, and we compared the estimated values ($\hat{R}_{RUP}$) to the actual values (R_{RUP}) in the flatfile. Starting with **M**, R_{JB}, and λ (the same inputs to SSC04), we determined the source parameters W, δ, Z_{TOR}, and α using the default estimation methods described above. For this testing dataset, the SSC04 methodology has a root mean squared error (*RMSE*) of 1.8 km, and our methodology has $RMSE = 1.5$ km, where

$$RMSE = \sqrt{\frac{1}{n} \sum_{i=1}^{n} \left[(R_{RUP})_i - (\hat{R}_{RUP})_i \right]^2}. \tag{22}$$

Although our method slightly out-performs the SSC04 method, this is not a significant difference in performance; both methods perform well. If the objective were to simply estimate R_{RUP} from R_{JB} and end there, then the SSC04 method is adequate. However, when R_X is also needed (as in the AS08 and CY08 models), our method is advantageous, because R_X

cannot be estimated using the SSC04 relationships. One other potential issue is that the SSC04 equations are technically only applicable for $R_{JB} \leq 100$ km, whereas our equations are physically derived and are applicable for any distance range at which the flat-earth assumption is valid (typically, several hundred kilometers). Note, however, that at large distances from the earthquake source, the values of R_{JB} and R_{RUP} converge; the distinction is more important at small distances.

ESTIMATION OF SITE PARAMETERS

The time-averaged shear-wave velocity over a subsurface depth of 30 meters (V_{S30}) is the primary site characteristic in each of the NGA models except for I08, which does not explicitly include site response. Our framework requires that the user assume a value of V_{S30}. At locations without measured shear-wave velocity profiles, the user may turn to published correlations of V_{S30} with surficial geology (Wills and Clahan 2006), topographic slope (Wald and Allen 2007), and other geotechnical information (Dobry et al. 2000). Alternatively, estimates of V_{S30} at unsampled locations may be obtained by geostatistical approaches, such as the spatial interpolation schemes described by Thompson et al. (2010). Although estimates of V_{S30} are included for nearly every station in the NGA flatfile, the depth parameters $Z_{1.0}$ and $Z_{2.5}$ are not present for many records. For the common situation in which a site-specific V_S profile is not available, the next priority would be to obtain the depth parameters from a regional velocity model, such as that of Tinsley and Fumal (1985) for the Los Angeles Basin and Holzer et al. (2005) for the San Francisco Bay Area. If a regional velocity model is not available, the methodology in the following paragraphs (suggested by the model developers) may be used for estimating the depth parameters. Another possible method is to apply the technique outlined in Douglas et al. (2009) to estimate V_S profiles based on the information available, and then compute V_{S30}, $Z_{1.0}$, and $Z_{2.5}$ as needed from the estimated profile.

DEPTH TO $V_S = 1.0$ km/s, $Z_{1.0}$

To estimate $Z_{1.0}$ when applying the AS08 and CY08 models, users should follow recommendations of the respective model developers. Abrahamson and Silva (2008) recommend using the following median relationship to estimate $Z_{1.0}$ (m) from V_{S30} (m/s):

$$Z_{1.0} = \begin{cases} \exp(6.745) & \text{for } V_{S30} < 180 \,\text{m/s} \\ \exp\left[6.745 - 1.35 \cdot \ln\left(\dfrac{V_{S30}}{180}\right)\right] & \text{for } 180 \leq V_{S30} \leq 500 \,\text{m/s} \\ \exp\left[5.394 - 4.48 \cdot \ln\left(\dfrac{V_{S30}}{500}\right)\right] & \text{for } V_{S30} > 500 \,\text{m/s}. \end{cases} \tag{23}$$

Chiou and Youngs (2008a) recommend using the following median relationship to estimate $Z_{1.0}$ from V_{S30}:

$$Z_{1.0} = \exp\left[28.5 - \frac{3.82}{8} \cdot \ln\left(V_{S30}{}^8 + 378.7^8\right)\right]. \tag{24}$$

The AS08 model was derived so that Equation 23 should be used when $Z_{1.0}$ is unknown, and the CY08 model was derived so that Equation 24 should be used for estimating $Z_{1.0}$. Thus, although this requires having two separate estimates of $Z_{1.0}$ for a single site, Equation 23 should be used when estimating $Z_{1.0}$ for the AS08 model, and Equation 24 should be used when estimating $Z_{1.0}$ for the CY08 model. The estimated values of $Z_{1.0}$ are different for Equations 23 and 24 because of differences in the functional forms and in the datasets used to develop the equations. Abrahamson and Silva (2008) developed Equation 23 from analytical site response models, and Chiou and Youngs (2008b) developed Equation 24 using an updated velocity model for southern California, which has smaller depth parameters than the previous velocity model reflected in the NGA flatfile. However, as discussed in Kaklamanos and Baise (2011), these relationships display a high degree of scatter, as it is inherently difficult to use V_{S30} to estimate a parameter that typically involves depths much greater than 30 m.

DEPTH TO $V_S = 2.5$ km/s, $Z_{2.5}$

In order to estimate $Z_{2.5}$, Campbell and Bozorgnia (2007) offer guidelines for extrapolating the estimates of $Z_{1.0}$ or $Z_{1.5}$ (depth to $V_S = 1.5$ km/s) if these values are available. If $Z_{1.5}$ is known, then the following equation may be used to estimate $Z_{2.5}$, where all depths are in meters:

$$Z_{2.5} = 636 + 1.549Z_{1.5}. \tag{25}$$

If $Z_{1.0}$ is known (but $Z_{1.5}$ is unknown), then $Z_{2.5}$ may be estimated by the following extrapolation:

$$Z_{2.5} = 519 + 3.595Z_{1.0}. \tag{26}$$

When $Z_{1.0}$ is unknown, the AS08 equation for $Z_{1.0}$ (Equation 23) may be used to estimate $Z_{1.0}$ from V_{S30}, and $Z_{2.5}$ may then be obtained from Equation 26. Equation 23 (AS08) is used instead of Equation 24 (CY08) because the depth dependence of CB08 is based on an earlier version of the velocity model than the version Chiou and Youngs (2008b) used to develop Equation 24.

CONCLUSIONS

We have developed a straightforward framework for implementing the ground-motion prediction equations developed as part of the Next Generation Attenuation of Ground Motions (NGA-West) project in 2008. Using our methodology, users can employ the NGA models knowing only the earthquake magnitude, style of faulting, one distance measure, average shear-wave velocity of the site, and the hanging-wall flag. We have offered a comprehensive summary of recommendations and alternatives for estimating the various source, path, and site parameters. Using various geometric principles, we have derived physical equations relating the three distance measures found in the NGA models (R_{JB}, R_{RUP}, and R_X). For models with multiple distance parameters, the geometric interdependence of the distance parameters is a phenomenon that must be considered in model implementation, especially at small source-to-site distances. The publication of these equations will save users the need to repeat the derivations, some of which are quite complicated. Our framework will

allow the NGA models to become more accessible to members of the earthquake engineering community, and may help with the implementation of other present or future GMPEs.

ACKNOWLEDGMENTS

REFERENCES

Abrahamson, N., Atkinson, G., Boore, D., Bozorgnia, Y., Campbell, K., Chiou, B., Idriss, I. M., Silva, W., and Youngs, R., 2008. Comparisons of the NGA ground-motion relations, *Earthquake Spectra* **24**, 45–66.

Abrahamson, N. A., and Silva, W. J., 2008. Summary of the Abrahamson & Silva NGA ground-motion relations, *Earthquake Spectra* **24**, 67–97.

Bommer, J. J., Scherbaum, F., Bungum, H., Cotton, F., Sabetta, F., and Abrahamson, N. A., 2005. On the use of logic trees for ground-motion prediction equations in seismic-hazard analysis, *Bulletin of the Seismological Society of America* **95**, 377–389.

Boore, D. M., and Atkinson, G. M., 2008. Ground-motion prediction equations for the average horizontal component of PGA, PGV, and 5%-damped PSA at spectral periods between 0.01 s and 10.0 s, *Earthquake Spectra* **24**, 99–138.

Campbell, K. W., and Bozorgnia, Y., 2006. Next Generation Attenuation (NGA) empirical ground motion models: Can they be used in Europe?, in *Proceedings, First European Conference on Earthquake Engineering and Seismology*, Paper 458, Geneva, Switzerland.

Campbell, K. W., and Bozorgnia, Y., 2007. Campbell-Bozorgnia NGA ground motion relations for the geometric mean horizontal component of peak and spectral ground motion parameters, *PEER Report No. 2007/02*, Pacific Earthquake Engineering Research Center, University of California, Berkeley.

Campbell, K. W., and Bozorgnia, Y., 2008. NGA ground motion model for the geometric mean horizontal component of PGA, PGV, PGD and 5% damped linear elastic response spectra for periods ranging from 0.01 to 10 s, *Earthquake Spectra* **24**, 139–171.

Chiou, B. S.-J., 2005. Documentation for NGA flatfile used for development of NGA models, Pacific Earthquake Engineering Research Center, University of California, Berkeley, http://peer.berkeley.edu/nga/NGA_Documentation.pdf, last accessed August 2011.

Chiou, B. S.-J., and Youngs, R. R., 2008a. An NGA model for the average horizontal component of peak ground motion and response spectra, *Earthquake Spectra* **24**, 173–215.

Chiou, B. S.-J., and Youngs, R. R., 2008b. NGA model for the average horizontal component of peak ground motion and response spectra, *PEER Report No. 2008/09*, Pacific Earthquake Engineering Research Center, University of California, Berkeley.

Collettini, C., and Sibson, R. H., 2001. Normal faults, normal friction?, *Geology* **29**, 927–930.

Dobry, R., Borcherdt, R. D., Crouse, C. B., Idriss, I. M., Joyner, W. B., Martin, G. R., Power, M. S., Rinne, E. E., and Seed, R. B., 2000. New site coefficients and site classification system used in recent building seismic code provisions, *Earthquake Spectra* **16**, 41–67.

Douglas, J., 2003. Earthquake ground motion estimation using strong-motion records: a review of equations for the estimation of peak ground acceleration and response spectral ordinates, *Earth Science Reviews* **61**, 43–104.

Douglas, J., Gehl, P., Bonilla, L. F., Scotti, O., Régnier, J., Duval, A.-M., and Bertrand, E., 2009. Making the most of available site information for empirical ground-motion prediction, *Bulletin of the Seismological Society of America* **99**, 1502–1520.

Ghasemi, H., Zare, M., and Fukushima, Y., 2008. Ranking of several ground-motion models for seismic hazard analysis in Iran, *Journal of Geophysics and Engineering* **5**, 301–310.

Holzer, T. L., Bennett, M. J., Noce, T. E., and Tinsley, J. C., 2005. Shear-wave velocity of surficial geologic sediments in northern California: statistical distributions and depth dependence, *Earthquake Spectra* **21**, 161–177.

Idriss, I. M., 2008. An NGA empirical model for estimating the horizontal spectral values generated by shallow crustal earthquakes, *Earthquake Spectra* **24**, 217–242.

Jackson, J. A., and White, N. J., 1989. Normal faulting in the upper continental crust: observations from regions of active extension, *Journal of Structural Geology* **11**, 15–36.

Kaklamanos, J., 2010. Implementation of the Kaklamanos et al. (2011) distance equations in Mathcad and Microsoft Excel, Department of Civil and Environmental Engineering, Tufts University, http://geohazards.cee.tufts.edu/people/jkakla01, last accessed August 2011.

Kaklamanos, J., and Baise, L. G., 2011. Model validations and comparisons of the Next Generation Attenuation of Ground Motions (NGA-West) project, *Bulletin of the Seismological Society of America* **101**, 160–175.

Kaklamanos, J., Boore, D. M., Thompson, E. M., and Campbell, K. W., 2010. Implementation of the Next Generation Attenuation (NGA) ground-motion prediction equations in Fortran and R, *U.S. Geological Survey Open-File Report 2010–1296*, Reston VA.

Mai, P. M., Spudich, P., and Boatwright, J., 2005. Hypocenter locations in finite-source rupture models, *Bulletin of the Seismological Society of America* **95**, 965–980.

Mai, P. M., 2007. Finite-source rupture model database, http://www.seismo.ethz.ch/srcmod/, last accessed August 2011.

Pacific Earthquake Engineering Research Center (PEER), 2008. Next Generation Attenuation of Ground Motions (NGA) project web site, http://peer.berkeley.edu/ngawest/index.html, last accessed August 2011.

R Development Core Team, 2011. *R: A Language and Environment for Statistical Computing*, R Foundation for Statistical Computing, Vienna, Austria, ISBN 3-900051-07-0, http://www.R-project.org, last accessed August 2011.

Scasserra, G., Stewart, J. P., Bazzurro, P., Lanzo, G., and Mollaioli, F., 2009. A comparison of NGA ground motion prediction equations to Italian data, *Bulletin of the Seismological Society of America* **99**, 2961–2978.

Scherbaum, F., Schmedes, J., and Cotton, F., 2004. On the conversion of source-to-site distance measures for extended earthquake source models, *Bulletin of the Seismological Society of America* **94**, 1053–1069.

Shoja-Taheri, J., Naserieh, S., and Ghofrani, H., 2010. A test of the applicability of NGA models to the strong ground motion data in the Iranian Plateau, *Journal of Earthquake Engineering* **14**, 278–292.

Sibson, R. H., and Xie, G., 1998. Dip range for intracontinental reverse fault ruptures: Truth not stranger than friction, *Bulletin of the Seismological Society of America* **88**, 1014–1022.

Spudich, P., and Chiou, B. S.-J., 2008. Directivity in NGA earthquake ground motions: Analysis using isochrone theory, *Earthquake Spectra* **24**, 279–298.

Stafford, P. J., Strasser, F. O., and Bommer, J. J., 2008. An evaluation of the applicability of the NGA models to ground-motion prediction in the Euro-Mediterranean region, *Bulletin of Earthquake Engineering* **6**, 149–177.

Tinsley, J. C., and Fumal, T. E., 1985. Mapping Quaternary sedimentary deposits for areal variations in shaking response, in *Evaluating Earthquake Hazards in the Los Angeles Region–-An Earth-Science Perspective*, *U. S. Geological Survey Professional Paper 1360* (J.I. Ziony, ed.), Washington, DC, 101–126.

Thompson, E. M., Baise, L. G., Kayen, R. E., Tanaka, Y., and Tanaka, H., 2010. A geostatistical approach to mapping site response spectral amplifications, *Engineering Geology* **114**, 330–342.

Wald, D. J., and Allen, T. I., 2007. Topographic slope as a proxy for seismic site conditions and amplification, *Bulletin of the Seismological Society of America* **97**, 1379–1395.

Wells, D. L., and Coppersmith, K. J., 1994. New empirical relationships among magnitude, rupture length, rupture width, rupture area, and surface displacement, *Bulletin of the Seismological Society of America* **84**, 974–1002.

Wills, C. J., and Clahan, K. B., 2006. Developing a map of geologically defined site-condition categories for California, *Bulletin of the Seismological Society of America* **96**, 1483–1501.